AAAS
Research
Volume 2020, Article ID 6727524, 8 pages
https://doi.org/10.34133/2020/6727524

Research Article

Asymmetric Schottky Contacts in van der Waals Metal-Semiconductor-Metal Structures Based on Two-Dimensional Janus Materials

Jia Liu,[1] Ji-Chang Ren,[1] Tao Shen,[1] Xinyi Liu,[1] Christopher J. Butch,[2,3] Shuang Li,[1] and Wei Liu[1]

[1]*Nano and Heterogeneous Materials Center, School of Materials Science and Engineering, Nanjing University of Science and Technology, Nanjing 210094, China*
[2]*Department of Biomedical Engineering, Nanjing University, Nanjing, China*
[3]*Blue Marble Space Institute of Science, Seattle, Washington, USA*

Correspondence should be addressed to Shuang Li; lishuang@njust.edu.cn and Wei Liu; weiliu@njust.edu.cn

Received 26 July 2020; Accepted 24 September 2020; Published 15 November 2020

Physical and electronic asymmetry plays a crucial role in rectifiers and other devices with a directionally variant current-voltage (I - V) ratio. Several strategies for practically creating asymmetry in nanoscale components have been demonstrated, but complex fabrication procedures, high cost, and incomplete mechanistic understanding have significantly limited large-scale applications of these components. In this work, we present density functional theory calculations which demonstrate asymmetric electronic properties in a metal-semiconductor-metal (MSM) interface composed of stacked van der Waals (vdW) heterostructures. Janus MoSSe has an intrinsic dipole due to its asymmetric structure and, consequently, can act as either an n-type or p-type diode depending on the face at the interior of the stacked structure (SeMoS-SMoS vs. SMoSe-SMoS). In each configuration, vdW forces dominate the interfacial interactions, and thus, Fermi level pinning is largely suppressed. Our transport calculations show that not only does the intrinsic dipole cause asymmetric I - V characteristics in the MSM structure but also that different transmission mechanisms are involved across the S-S (direct tunneling) and S-Se interface (thermionic excitation). This work illustrates a simple and practical method to introduce asymmetric Schottky barriers into an MSM structure and provides a conceptual framework which can be extended to other 2D Janus semiconductors.

1. Introduction

Physical and electronic asymmetry plays a crucial role in devices like rectifiers [1–4], which produce current-voltage (I - V) outputs and vary directionally depending on the applied bias. At the nanoscale, one strategy to produce current asymmetry is through metal-semiconductor-metal (MSM) structures composed of two metal-semiconductor (MS) junctions with distinct Schottky barriers connected back to back [5, 6]. In such an MSM, when a nonzero bias voltage is applied, one Schottky barrier is forward biased and the other one is reversed biased [6]. Compared to a single Schottky barrier MS diode, the second MS interface of the MSM diode further modulates current allowing backward current to also vary with voltage. An asymmetric MSM structure can be created by several strategies including using two electrodes with different work functions [7], asymmetric contact geometries [8], externally applied mechanical forces (*e.g.*, piezoelectric-potential-controlled Schottky diodes) [5], and enhanced metal oxidation or defect density differences [9]. However, large-scale application of these techniques is limited by high cost and difficulties in fabrication which include force-induced instability, shape selection, and Fermi level pinning (FLP) [8, 10]. Among these, FLP caused by defects is the most universal [7], can significantly hinder effective control of Schottky barriers at the contact, and requires complicated treatment of the bulk metal to avoid [11]. To overcome these obstacles, herein, we propose a new class of MSM structure fabricated by stacking two-dimensional (2D) Janus materials and 2D metals. Compared to other

approaches, fabrication of these MSMs is straightforward and effective since (1) the surface of these 2D materials is well controlled; (2) the dipole which generates the surface asymmetry is inherent to the Janus material (*e.g.*, MoSSe [12] and GeSe [13]); (3) the interface of the layered 2D materials is dominated by van der Waals (vdW) forces rather than chemical bonds, significantly suppressing the effect of FLP; and (4) asymmetric Schottky contacts can be created without requiring external forces, shape selection, doping, or precise control of contact geometries.

The term "Janus" is derived from the two-faced Roman god of transitions, and in nanotechnology, it refers to structures with two distinct faces, usually due to different terminating atoms on opposite surfaces [14, 15]. A large variety of 2D Janus materials have been predicted theoretically and/or fabricated experimentally [16–20]. Examples include Janus transition-metal dichalcogenides (TMDCs, such as MoSSe, WSSe, MoSTe, and WSTe) [16, 19, 21–29], Janus metal-nitrides and metal-carbides (MXenes, such as Cr_2COF and V_2COF) [14], Janus graphene [15, 18, 30], Janus black arsenic-phosphorus [31], Janus group-III chalcogenides (such as Ga_2SSe, In_2SSe, Ga_2STe, and In_2STe) [19, 32], and Janus group IV monochalcogenides (such as GeSe and SnS) [13, 33]. These asymmetric structures generate intrinsic electric fields (F) associated with the interior dipole across the plane, causing the two surfaces to have different work functions, and consequently, different Schottky barriers are generated dependent on the interfacial surface. On the basis of these observations, we hypothesized that when a Janus monolayer, such as MoSSe, is used as the semiconductor in MSM structures, the intrinsic dipole may introduce electronic asymmetry in a simple and practical manner.

In this contribution, we propose an asymmetric MSM design composed of layered Janus MoSSe and 1T-phase MoS_2. MoSSe has been fabricated experimentally, by substituting S (Se) atoms with Se (S) in the exposed surface of a MoS_2 ($MoSe_2$) monolayer [16, 22]. The metallic 1T-phase MoS_2 [34] was selected to avoid FLP problems associated with the use of bulk metals as contacts [7, 35, 36]. While metallic 1T MoS_2 [34] is dynamically instable, it has been demonstrated experimentally [37] and was selected, largely, as a prototype to demonstrate that FLP problems associated with the use of bulk metals as contacts can be avoided through employing 2D materials [7, 35, 36]. Our calculations predict different types of Schottky contacts at the interface of MoSSe/MoS_2 heterostructures: the n-type S-S interface and p-type S-Se interface. In both cases, the intrinsic dipole of MoSSe is preserved, while the FLP effects are significantly suppressed as the 2D materials are fully bonded and interact through van der Waals (vdW) forces [38, 39]. In this MSM structure, the asymmetric Schottky barriers originate from the reversal of the inherent electric field in Janus MoSSe, which always points from Se to S atoms. The carrier transports under positive and negative bias voltages are found to be dominated by thermionic excitation and tunneling, respectively, further underscoring the asymmetry of the structure. Although discussions of our findings are mainly based on MoSSe, the concepts that we outline here can be extended to other 2D Janus semiconductors.

2. Computational Methods

Geometry optimizations and electronic property calculations were performed using the Vienna Ab initio Simulation Package (VASP) [40, 41]. The generalized gradient approximation (GGA) with Perdew-Burke-Ernzerhof (PBE) algorithm [42] was selected as the exchange-correlation functional. The interaction between ionic core and valance electrons was described using the projector-augmented wave (PAW) method [43, 44]. The DFT+vdW method of Tkatchenko and Scheffler [45] was employed to account for long-range vdW interactions. The DFT+vdW method was constructed from mean-field electronic structure calculations and has been shown to perform well in describing vdW forces between 2D materials [46, 47]. An energy cutoff of 400 eV and a Monkhorst-Pack scheme with a k-point mesh of $9 \times 9 \times 1$ were employed to ensure accuracy. Structures were relaxed with energy change converged to 1×10^{-5} eV/cell in electronic self-consistency cycles and all forces smaller than 0.01 eV/Å in ionic relation loops. The vacuum width is larger than 15 Å in the z direction to avoid interaction between periodic slabs. When calculating the Schottky barriers ϕ_p and ϕ_n, the z axis is set to 150 Å. The I - V characteristics and other transport properties of the contacts were calculated using the nonequilibrium Green's function (NEGF) method within the frame of DFT, as implemented in the Atomistix ToolKit (ATK) package [48]. We used numerical linear combination of atomic orbitals (LCAO) basis sets in device calculations.

The optimized lattice constants a for Janus MoSSe and 1T MoS_2 are 3.23 and 3.13 Å, respectively, consistent with previous studies [16, 49, 50]. The Mo-S bond distance in 1T MoS_2 is 2.43 Å. In MoSSe, the bond distance of Mo-S slightly decreases to 2.41 Å while Mo-Se is 2.53 Å due to the larger radius of the Se atom. After stacking, the relaxed lattice constants, a_A and a_B, of contacts with the S-S (C_{S-S}) and S-Se ($C_{S\text{-}Se}$) interfaces are 3.21 and 3.20 Å, respectively, with a lattice mismatch $(a_{MoS2}\text{-}a_{MoSSe})/a_{MoS2} = 3.19\%$.

3. Results and Discussion

Our calculations show that MoSSe is a semiconductor with a direct band gap of 1.63 eV, consistent with the experimental optical gap (1.68 eV) [22], while 1T MoS_2 is a 2D metal (see Figure S1). As shown in Figure 1(a), the asymmetric MSM structure has two contacts, where both contacts C_{S-S} (right side) and $C_{S\text{-}Se}$ (left side) are vdW heterojunctions. Since C_{S-S} and $C_{S\text{-}Se}$ exhibit different Schottky barrier heights (SBHs), this sandwich structure yields an asymmetric I - V characteristic. Figure 1(b) shows that the forward current from drain to source I_{ds} (2.34×10^{-14} A under 0.40 V and 300 K) is one order of magnitude larger than the backward I_{ds} (3.10×10^{-15} A under 0.40 V and 300 K). Under positive V_{ds}, the electrons drift from source to drain through the n-type barrier of C_{S-S}, while the holes drift in the opposite direction and across the p-type barrier of $C_{S\text{-}Se}$. Under negative V_{ds}, barriers for both electrons and holes increase relative to under positive V_{ds}, as shown in the schematic band diagrams in Figure 1(b).

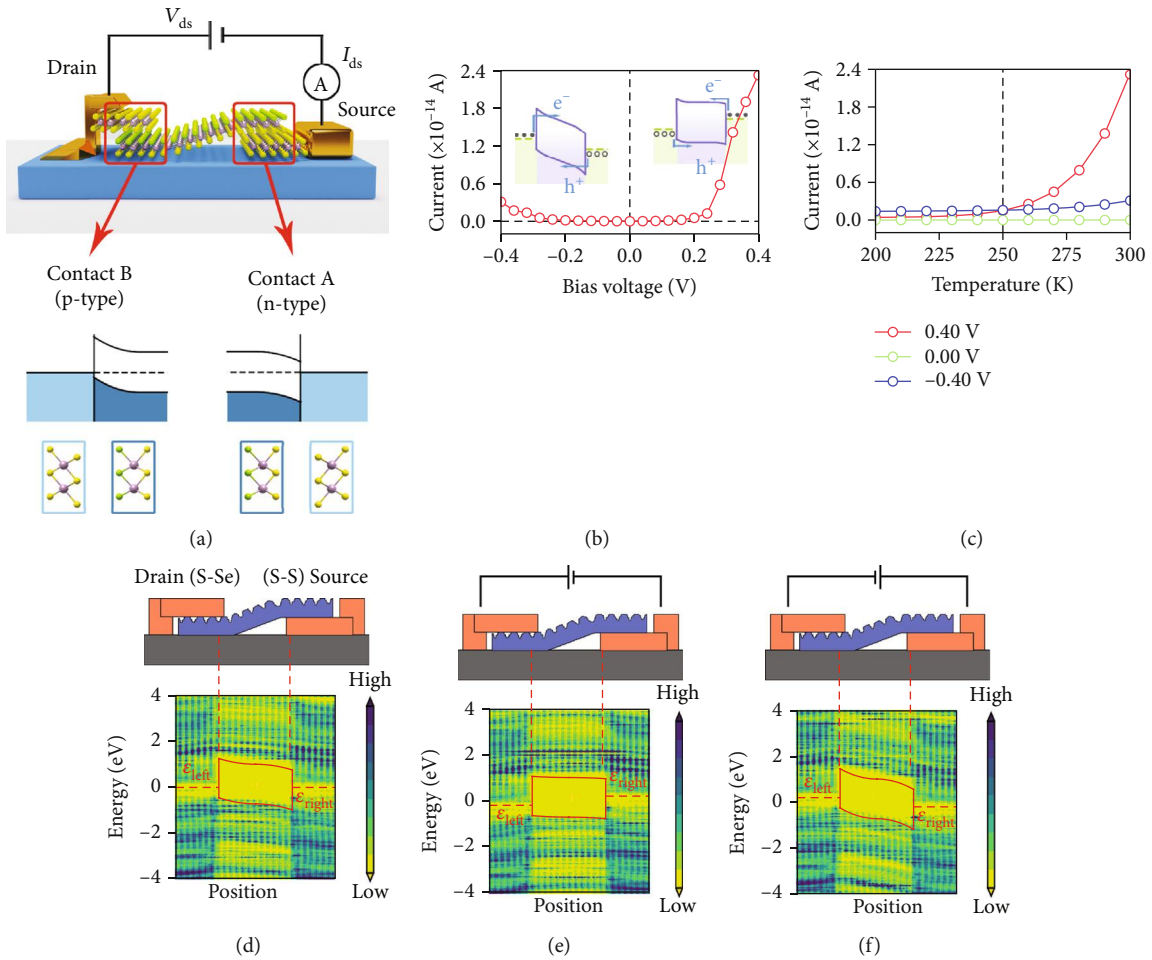

FIGURE 1: (a) Scheme of asymmetric van der Waals metal-semiconductor-metal diode based on two-dimensional Janus MoSSe (scattering region) and 1T MoS_2 (drain and source electrodes). The red squares indicate different contact interfaces with disparate Schottky barrier heights and band bending directions (S-S contact at source side with an n-type barrier and S-Se contact at drain side with a p-type barrier, marked as C_{S-S} and C_{S-Se}, respectively). The violet, yellow, and green spheres represent Mo, S, and Se atoms, respectively. (b) The corresponding I - V characteristic curve at 300 K of this device. The illustrations are schematic band diagrams under negative (left) and positive (right) bias voltages, respectively. The purple curves represent the boundary of electrodes and bending of CB and VB. The blue arrows represent the primary transferring methods through contacts (tunneling and thermionic excitation under negative and positive voltages, respectively). The green dashed lines indicate the Fermi levels in two electrodes. The hollow and stuffed circles denote holes and electrons, respectively. (c) The current versus temperature from 200 to 300 K of the MSM structure under different bias voltages. The vertical dashed line represents the critical temperature where red and blue curves are crossed around 250 K. (d)-(f) The spatially resolved local density of states (LDOS) projected on the position of contact under $V_{ds} = 0.00$, 0.40, and −0.40 V. The horizontal red dashed lines represent the chemical potentials (ε) of electrodes. The red curves illustrate the boundaries of electrodes and theoretical band diagrams. The device configurations are depicted above LDOS graphs for references. The orange squares represent 1T MoS_2, while the blue layer with one side flat and the other side fluctuant represents the Janus MoSSe semiconductor. The "S-S" and "S-Se" tags indicate C_{S-S} and C_{S-Se}, respectively.

Figure 1(c) shows that under negative V_{ds}, the I_{ds} varies slightly with increasing temperature (T). Under positive bias, I_{ds} has a much greater sensitivity to temperature. These results suggest different transport mechanisms between the two directions. To discern the transport mechanisms contributing to the current under each condition, we plotted the spatially resolved local density of states (LDOS) along the transport direction under $V_{ds} = 0$ and ± 0.40 V (Figure 1(d)–1(f)). The flat conduction band (CB) and valence band (VB) at the metal-semiconductor interface (right illustration in Figures 1(b) and 1(e)), along with the exponential I - V curve (Figure 1(b)), indicate that carrier transport under positive bias voltages is mainly through thermionic excitation [51, 52]. In contrast, the CB and VB near the interface bend downward with the barrier becoming sharp under negative V_{ds} (Figure 1(b) left, and Figure 1(f)) leading to I_{ds}which appears to increase quadratically relative to V_{ds} (Figure 1(b)). These results illustrate that carrier transport in this case is consistent with the Fowler-Nordheim (F-N) model [53], implying it occurs mainly through a tunneling mechanism. In the F-N model, $I(V) \propto V^2 \exp\left(-4d_\phi\sqrt{2m^*\phi^3}/(3\hbar qV)\right)$ [53, 54], where $\hbar$ is the reduced Planck constant, m^* is the effective mass of carrier

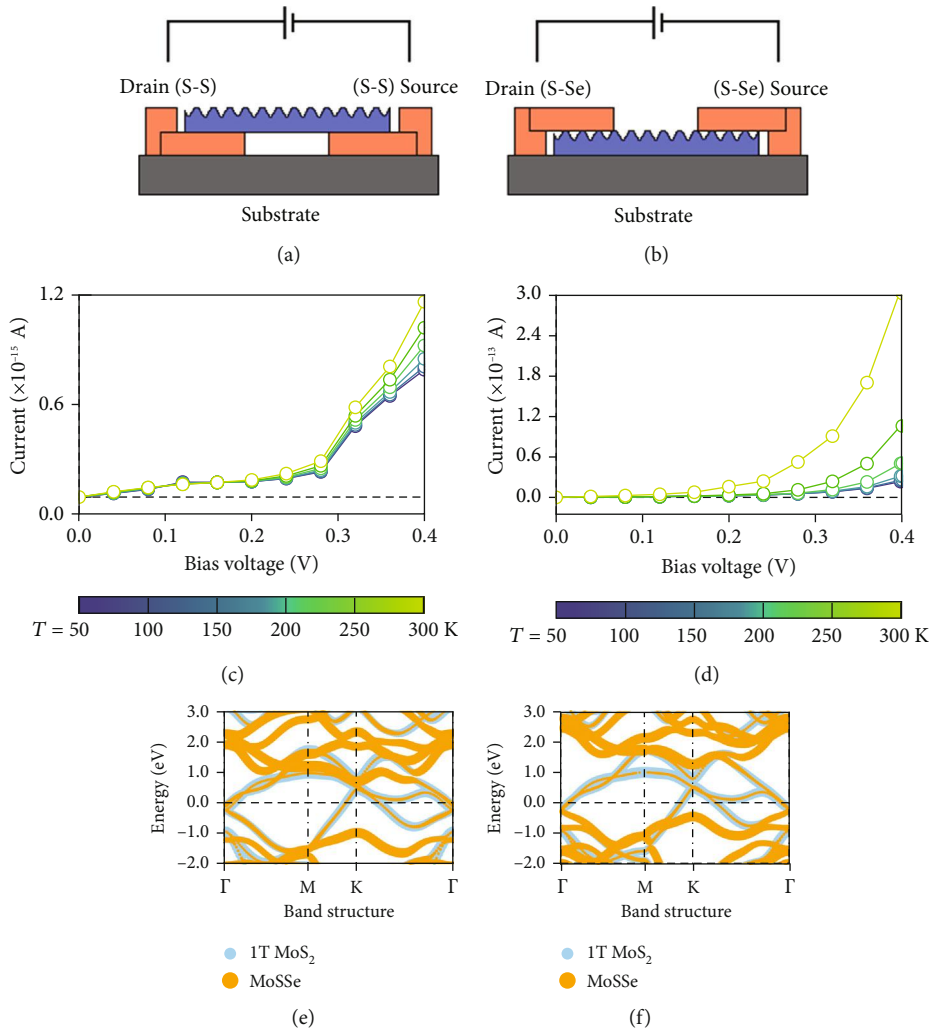

FIGURE 2: (a), (b) The symmetric devices made from C_{S-S} and C_{S-Se} and marked as D_{S-S} and D_{S-Se}, respectively. (c), (d) The I - V characteristic curves under different temperatures of D_{S-S} and D_{S-Se}, respectively. The electrode temperatures are ranged from 50 to 300 K. The bias voltages are ranged from 0.00 to 0.40 V because the I - V curves under positive and negative bias are symmetric. Note that the current in two devices is in different orders of magnitudes due to disparate transmission mechanisms. (e), (f) The projected band structures of C_{S-S} and C_{S-Se}, respectively. The sizes of the blue and orange dots represent the relative weights of 1T MoS_2 and Janus MoSSe layers, respectively.

in system, and d_ϕ is the barrier width. These trends show that forward conduction in the MSM occurs through thermionic excitation while back-current occurs through F-N tunneling. Due to these different mechanisms, the scaling of these effects with temperature varies, yielding a temperature critical point (T_0) around 250 K where the preferred direction of conduction inverts at T_0 (when $T < T_0, I_{ds}(0.40\,\text{V}) < I_{ds}(-0.40\,\text{V})$, while it reversed when $T > T_0$). Consequently, the temperature dependence of thermionic transport has a key influence on the rectification properties of the MSM.

Given that each MS junction contributes to the overall device performance, we constructed two conventional symmetric MSM structures composed of two of each interface (S-S in Figure 2(a) and S-Se in Figure 2(b)) for comparison to the asymmetric device discussed above. Like the asymmetric MSM structure, the electrode and central region lengths for these devices were set to 5.55 and 66.64 Å, respectively, for D_{S-S} (*i.e.*, symmetric device made from two C_{S-S}) and 5.55 and 66.57 Å, respectively, for D_{S-Se} (device with two C_{S-Se}). As expected, the computed I - V curves exhibit a diode-like feature for both D_{S-S} and D_{S-Se} under positive V_{ds} from 0.00 to 0.40 V. In contrast to the asymmetric counterparts, D_{S-S} and D_{S-Se} display identical I - V curves under positive and negative voltage due to the symmetric band diagrams and identical transport mechanisms at the two interfaces. Because the current in D_{S-S} has only a weak dependence on T (Figure 2(c)), we speculated that the transmission in D_{S-S} is dominated by direct quantum tunneling. Unlike F-N tunneling, the direct tunneling model predicts I_{ds} to vary linearly with V_{ds} $I(V) \propto V \exp\left(-2d_\phi\sqrt{2m^*\phi}/\hbar\right)$ [53, 54]. Above 0.30 V, however, F-N tunneling does occur, as shown in Figure 2(c) and Figure S2. In contrast, I_{ds} in D_{S-Se} (Figure 2(d)) has exponential temperature dependence, increasing by a factor of 10 between 50 and 300 K, suggesting thermionic excitation to be the main transport mechanism. Under the same conditions, the current I_{ds} in D_{S-S} (0.40 V,

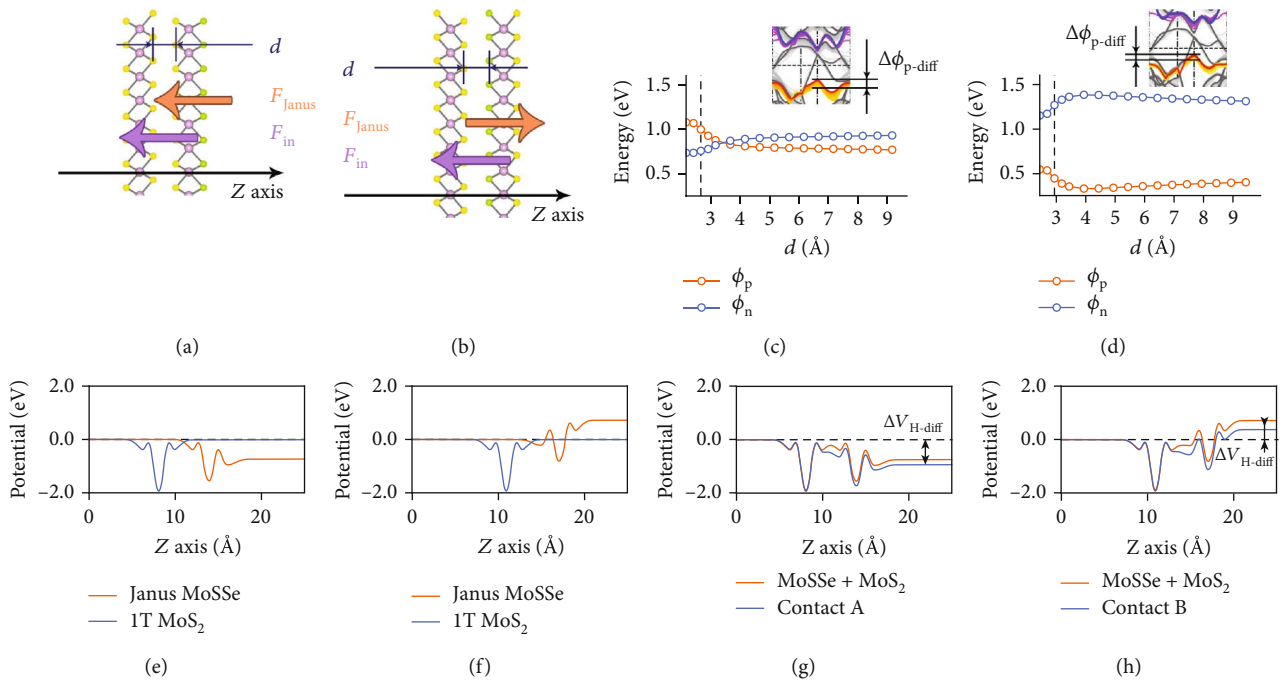

FIGURE 3: (a), (b) Schematic diagrams of electric field screening effect combined with intrinsic (orange arrows) and interfacial F (purple arrows) in contacts with S-S (C_{S-S}) and S-Se (C_{S-Se}) interfaces, respectively. The z axis perpendicular to the plane is corresponding to the abscissas of subplots (e)-(h). (c), (d) The ϕ_p and ϕ_n of C_{S-S} and C_{S-Se} under different d. The vertical grey dashed lines indicate the d in balanced states. The illustrations are corresponding band structures of contacts at different d. The yellow to red and purple to blue lines indicate the movements of VB and CB of Janus MoSSe. The arrows and tags $\Delta\phi_{p-diff}$ indicate the p-type barrier differences. (e), (f) The separated $\Delta V_{H-MoSSe}$ and ΔV_{H-MoS2} of monolayers in C_{S-S} and C_{S-Se} versus z position, respectively. (g), (h) The $\Delta V_{H-MoSSe} + \Delta V_{H-MoS2}$ and $\Delta V_{H-total}$ of C_{S-S} and C_{S-Se} versus z position, respectively. The arrows in plot (g) and (h) indicate the differences of electrostatic potentials from metal to semiconductor (ΔV_{H-diff}).

300 K) is 1.16×10^{-15} A, which is about two orders of magnitude lower than D_{S-Se} (3.08×10^{-13} A (0.40 V, 300 K)).

The differences in the current and temperature dependence above show that C_{S-S} and C_{S-Se} have markedly different transmission mechanisms and magnitudes and the order of their assembly controls the properties of the resultant device. To understand the physical origins of these differences between the two junctions, we plotted the band structures of C_{S-S} and C_{S-Se} (Figures 2(e) and 2(f)). These band structures show that the metallic properties of 1T MoS_2 are well preserved in C_{S-S} and C_{S-Se}. Further, the band structure of MoSSe is almost unchanged relative to the isolated monolayer band structure (Figure S1). These largely retained band configurations, interlayer distances typical of vdW interactions, and weak adsorption energies clearly suggest that the interactions between the two layers are dominated by the vdW forces. This vdW interface effectively suppresses the FLP effect, due to the reduction of localized densities of states at the interface, metal-induced gap states, and defect/disorder-induced gap states [38, 55, 56].

Schottky barrier heights ϕ_n and ϕ_p can be calculated from band structures of the metal-semiconductor junction using the following equations [13, 57]:

$$\phi_n = E_{CBM} - E_F, \tag{1}$$

$$\phi_P = E_F - E_{VBM}, \tag{2}$$

where E_F is the Fermi level of the junction, while E_{CBM} and E_{VBM} are the CBM and VBM energies of the 2D semiconductor in contact. According to Eqs. (1) and (2), C_{S-S} is an n-type Schottky contact (ϕ_n and ϕ_p are 0.76 and 0.98 eV, respectively) with bands bending downward slightly, while C_{S-Se} is a p-type Schottky contact (ϕ_n and ϕ_p are 1.26 and 0.45 eV, respectively) with significant upward bending at the metal-semiconductor interface. Notably, although vdW forces dominate the metal-semiconductor interaction, ϕ_n and ϕ_p still deviate from the Schottky-Mott rule [58]:

$$\phi_n' = W_{metal} - \chi, \tag{3}$$

where W_{metal} and χ are the work function and electron affinity of 1T MoS_2 and Janus MoSSe. From equation (3), the idealized Schottky barrier (ϕ_n') would be expected to be 0.84 eV.

The deviation from the ideal Schottky barrier is likely due to the contribution of the inherent field of Janus MoSSe (F_{Janus}) along with the two interfacial dipoles ($F_{in,S-S}$, $F_{in,S-Se}$). To determine the degree to which each of these elements affects the deviation, we separated the two layers of C_{s-s} and C_{S-Se} and measured the variation of ϕ_n and ϕ_p (Figures 3(a) and 3(b)). These calculations show the interface dipole decreases rapidly

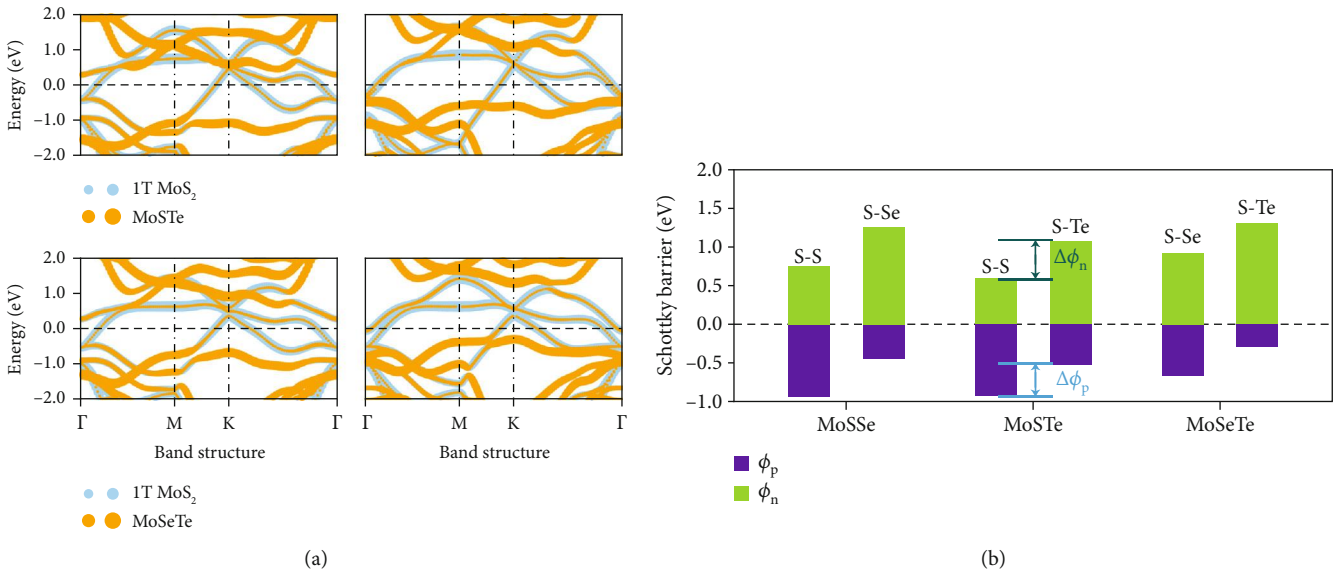

FIGURE 4: (a) The projected band structures of bilayer 1T MoS_2-MoSTe with S-S (upper left) and S-Te (upper right) interfaces and 1T MoS_2-MoSeTe with S-Se (lower left) and S-Te (lower right) interfaces. (b) The asymmetric Schottky barriers of Janus MoSSe, MoSTe, and MoSeTe contacting with metal 1T MoS_2. The text above each volume indicates the contact interface, where each Janus material has two different contact interfaces. The tags $\Delta\phi_p$ and $\Delta\phi_n$ are p-type and n-type Schottky barrier differences between two interfaces.

and that the effect can be ignored at distances larger than 5 Å based on the near-total reversion of the material bands back to their isolated states. To ensure no interaction between systems, the z period was set to 150 Å (sensitivity analysis in Figure S3). Interestingly, both $C_{S\text{-}S}$ and $C_{S\text{-}Se}$ become p-type when $d > 5$ Å and ϕ_p converge to 0.77 and 0.39 eV, respectively (Figures 3(c) and 3(d)), with the two interfaces being equivalent at 3.28 Å where $C_{S\text{-}S}$ transforms from p-type to an n-type structure.

Both F_{Janus} and F_{in} can contribute to the changes in the Schottky barrier with distance. The magnitude of these effects can be spatially resolved using the Hartree difference potential (ΔV_H) calculated as follows:

$$\Delta V_H = V_{total} - \sum V_{atom}, \tag{4}$$

where V_{total} and V_{atom} represent the Hartree potentials of system and each atom. Figures 3(e) and 3(f) show the ΔV_H MoSSe and 1T MoS_2 averaged in the plane along the z-axis according to Eq. (4) clearly indicating F_{Janus} directs from Se to S atoms (orange arrows in Figures 3(a) and 3(b)) in agreement with previous studies [17]. This results in lower electrostatic potential at the MoSSe side of $C_{S\text{-}S}$ and higher potential for the MoSSe side of $C_{S\text{-}Se}$, an effect which will naturally perturb the Schottky barrier height. In contrast, Figures 3(g) and 3(h) show the sum of the plane averaged ΔV_H of the isolated systems (orange lines) as compared to the assembled contacts. In each case, the difference between the isolated and assembled systems corresponds to the effect of F_{in}. Figure 3(g) shows $F_{in,S\text{-}S}$ to be oriented with F_{Janus}, pointing from MoSSe to 1T MoS_2, and increasing the electrostatic potential from metal to semiconductor ($\Delta V_{H\text{-}diff}$). Inversely, $F_{in,S\text{-}Se}$ and F_{Janus} have opposite direction, reducing the apparent magnitude of F_{Janus} and decreasing $\Delta V_{H\text{-}diff}$ (Figure 3(h)). These $\Delta V_{H\text{-}diff}$ calculations are consistent with the deviations from the ideal Schottky barrier and demonstrate how the synergistic effect of F_{Janus} and F_{in} govern the electronic properties of $C_{S\text{-}S}$ and $C_{S\text{-}Se}$. The large $\Delta V_{H\text{-}diff}$ on the sulfur side of MoSSe will cause a greater barrier difference in $C_{S\text{-}S}$ ($\Delta\phi_{p\text{-}diff} = 0.31$ eV) while the smaller $\Delta V_{H\text{-}diff}$ on the Se side leads to less deviation in $C_{S\text{-}Se}$ ($\Delta\phi_{p\text{-}diff} = 0.14$ eV) This also rationalizes the transition of $C_{S\text{-}S}$ from p-type to n-type at $d \approx 3.28$ Å as the synergistic effect abates.

Finally, to generalize our proposed approach to other 2D Janus materials, we calculated the Schottky barriers in the two sides of Janus MoSTe and MoSeTe contacted with 1T MoS_2 (Figure S4). Both their projected band structures (Figure 4(a)) and barriers ϕ_p and ϕ_n (Figure 4(b)) indicate these Janus MSMs to also exhibit asymmetric SBHs. Notably, while Janus MoSSe would generate the largest $\Delta\phi_p$ ($\Delta\phi_n$) among these three structures, the relationship is not linear with the vacuum level shifts of the free-standing Janus layers $\Delta E_{vac\text{-}MoSTe} > \Delta E_{vac\text{-}MoSSe} > \Delta E_{vac\text{-}MoSeTe}$ [21]. This initial result shows how the dipole of a Janus structure, the initial work function, and charge transfer also have a great influence on the asymmetry of barriers.

4. Conclusions

We demonstrate that 1T MoS_2 and Janus MoSSe can form an asymmetric van der Waals MSM device with two different barriers contacted back to back through reversing the intrinsic dipole of Janus MoSSe. The transmissions in this MSM device under positive and negative V_{ds} are dominated by thermionic excitation and tunneling, respectively, and the rectifying directions and ratios could be effectively controlled by temperature. Furthermore, through the calculations of the differences of electrostatic potentials, we found that the

rectifying behaviors hugely associate with the interaction between the intrinsic electric field of the Janus layer and the field induced at the interface. The asymmetric Schottky barrier heights inherent to this design are caused by the intrinsic field of the Janus semiconductor, meaning there is ample room to explore other 2D metals in the search for new MSM devices and the design of "all-2D" flexible high-performance rectifiers.

Conflicts of Interest

The authors declare no competing financial interest.

Acknowledgments

We acknowledge supports from the NSF of China (51722102, 21773120, 51602155), the NSF of Jiangsu Province (BK20180448), the Fundamental Research Funds for the Central Universities (30920041116, 30920021159, 30919011405), and Jiangsu Key Laboratory of Advanced Micro&Nano Materials and Technology.

Supplementary Materials

The atomic structures and band structures of Janus MoSSe and 1T MoS_2, respectively; the plotted ln (I/V^2) *vs.* ln ($1/V$) and $1/V$ for D_{S-S}; the ϕ_p and ϕ_n movements at K point of C_{S-S} and C_{S-Se}; the vdW contact structures of Janus MoSTe (or MoSeTe) and 1T MoS_2. *(Supplementary Materials)*

References

[1] A. Di Bartolomeo, "Graphene Schottky diodes: an experimental review of the rectifying graphene/semiconductor heterojunction," *Physics Reports*, vol. 606, no. 1, pp. 1–58, 2016.

[2] J.-Y. Wu, Y. T. Chun, S. Li, T. Zhang, and D. Chu, "Electrical rectifying and photosensing property of Schottky diode based on MoS_2," *ACS Applied Materials & Interfaces*, vol. 10, no. 29, pp. 24613–24619, 2018.

[3] X. X. Li, Z. Q. Fan, P. Z. Liu et al., "Gate-controlled reversible rectifying behaviour in tunnel contacted atomically-thin MoS_2 transistor," *Nature Communications*, vol. 8, no. 1, p. 970, 2017.

[4] K. Murali, M. Dandu, S. Das, and K. Majumdar, "Gate-tunable WSe2/SnSe2Backward diode with ultrahigh-reverse rectification ratio," *ACS Applied Materials & Interfaces*, vol. 10, no. 6, pp. 5657–5664, 2018.

[5] J. Zhou, P. Fei, Y. Gu et al., "Piezoelectric-potential-controlled polarity-reversible Schottky diodes and switches of ZnO wires," *Nano Letters*, vol. 8, no. 11, pp. 3973–3977, 2008.

[6] S. M. Sze, D. J. Coleman Jr., and A. Loya, "Current transport in metal-semiconductor-metal (MSM) structures," *Solid State Electronics*, vol. 14, no. 12, pp. 1209–1218, 1971.

[7] J. Kang, W. Liu, D. Sarkar, D. Jena, and K. Banerjee, "Computational study of metal contacts to monolayer transition-metal dichalcogenide semiconductors," *Physical Review X*, vol. 4, no. 3, p. 14, 2014.

[8] C. Zhou, S. Raju, B. Li, M. Chan, Y. Chai, and C. Y. Yang, "Self-driven metal–semiconductor–metal WSe2Photodetector with asymmetric contact geometries," *Advanced Functional Materials*, vol. 28, no. 45, article 1802954, 2018.

[9] A. di Bartolomeo, A. Grillo, F. Urban et al., "Asymmetric schottky contacts in bilayer MoS_2 Field effect transistors," *Advanced Functional Materials*, vol. 28, no. 28, article 1800657, 2018.

[10] M. Fontana, T. Deppe, A. K. Boyd et al., "Electron-hole transport and photovoltaic effect in gated MoS_2 Schottky junctions," *Scientific Reports*, vol. 3, no. 1, article 1634, 2013.

[11] Y. Liu, J. Guo, E. Zhu et al., "Approaching the Schottky–Mott limit in van der Waals metal–semiconductor junctions," *Nature*, vol. 557, no. 7707, pp. 696–700, 2018.

[12] Y. Li, J. Wang, B. Zhou et al., "Tunable interlayer coupling and Schottky barrier in graphene and Janus MoSSe heterostructures by applying an external field," *Physical Chemistry Chemical Physics*, vol. 20, no. 37, pp. 24109–24116, 2018.

[13] L. Peng, Y. Cui, L. Sun et al., "Dipole controlled Schottky barrier in the blue-phosphorene-phase of GeSe based van der Waals heterostructures," *Nanoscale Horiz*, vol. 4, no. 2, pp. 480–489, 2019.

[14] N. C. Frey, A. Bandyopadhyay, H. Kumar, B. Anasori, Y. Gogotsi, and V. B. Shenoy, "Surface-engineered MXenes: electric field control of magnetism and enhanced magnetic anisotropy," *ACS Nano*, vol. 13, no. 3, pp. 2831–2839, 2019.

[15] L. Zhang, J. Yu, M. Yang, Q. Xie, H. Peng, and Z. Liu, "Janus graphene from asymmetric two-dimensional chemistry," *Nature Communications*, vol. 4, no. 1, article 1443, 2013.

[16] J. Zhang, S. Jia, I. Kholmanov et al., "Janus monolayer transition-metal dichalcogenides," *ACS Nano*, vol. 11, no. 8, pp. 8192–8198, 2017.

[17] F. Li, W. Wei, H. Wang, B. Huang, Y. Dai, and T. Jacob, "Intrinsic electric field-induced properties in Janus MoSSe van der Waals structures," *Journal of Physical Chemistry Letters*, vol. 10, no. 3, pp. 559–565, 2019.

[18] I. Jeon, M. D. Peeks, S. Savagatrup et al., "Janus graphene: scalable self-assembly and solution-phase orthogonal functionalization," *Advanced Materials*, vol. 31, no. 21, article 1900438, 2019.

[19] R. Li, Y. Cheng, and W. Huang, "Recent progress of Janus 2D transition metal chalcogenides: from theory to experiments," *Small*, vol. 14, no. 45, article 1802091, 2018.

[20] M. Yagmurcukardes, Y. Qin, S. Ozen et al., "Quantum properties and applications of 2D Janus crystals and their superlattices," *Applied Physics Reviews*, vol. 7, no. 1, article 011311, 2020.

[21] A. C. Riis-Jensen, T. Deilmann, T. Olsen, and K. S. Thygesen, "Classifying the electronic and optical properties of Janus monolayers," *ACS Nano*, vol. 13, no. 11, pp. 13354–13364, 2019.

[22] A.-Y. Lu, H. Zhu, J. Xiao et al., "Janus monolayers of transition metal dichalcogenides," *Nature Nanotechnology*, vol. 12, no. 8, pp. 744–749, 2017.

[23] W. Chen, X. Hou, X. Shi, and H. Pan, "Two-dimensional Janus transition metal oxides and chalcogenides: multifunctional properties for photocatalysts, electronics, and energy conversion," *ACS Applied Materials & Interfaces*, vol. 10, no. 41, pp. 35289–35295, 2018.

[24] H. Jin, T. Wang, Z.-R. Gong, C. Long, and Y. Dai, "Prediction of an extremely long exciton lifetime in a Janus-MoSTe monolayer," *Nanoscale*, vol. 10, no. 41, pp. 19310–19315, 2018.

[25] A. Kandemir and H. Sahin, "Bilayers of Janus WSSe: monitoring the stacking type via the vibrational spectrum," *Physical*

Chemistry Chemical Physics, vol. 20, no. 25, pp. 17380–17386, 2018.

[26] Z. Wang, "2H →1T′ phase transformation in Janus monolayer MoSSe and MoSTe: an efficient hole injection contact for 2H-MoS_2," *Journal of Materials Chemistry C*, vol. 6, no. 47, pp. 13000–13005, 2018.

[27] C. Jin, X. Tang, X. Tan, S. C. Smith, Y. Dai, and L. Kou, "A Janus MoSSe monolayer: a superior and strain-sensitive gas sensing material," *Journal of Materials Chemistry A*, vol. 7, no. 3, pp. 1099–1106, 2019.

[28] A. Bafekry, M. Yagmurcukardes, B. Akgenc, M. Ghergherehchi, and C. V. Nguyen, "Van der Waals heterostructures of MoS_2 and Janus MoSSe monolayers on graphitic boron-carbon-nitride (BC_3, C_3N, C_3N_4 and C_4N_3) nanosheets: a first-principles study," *Journal of Physics D: Applied Physics*, vol. 53, no. 35, article 355106, 2020.

[29] M. Yagmurcukardes and F. M. Peeters, "Stable single layer of Janus MoSO: strong out-of-plane piezoelectricity," *Physical Review B*, vol. 101, no. 15, article 155205, 2020.

[30] X. F. Chen, Y. F. Zhu, and Q. Jiang, "Utilisation of Janus material for controllable formation of graphene p–n junctions and superlattices," *RSC Advances*, vol. 4, no. 8, pp. 4146–4154, 2014.

[31] L. L. Li, C. Bacaksiz, M. Nakhaee, R. Pentcheva, F. M. Peeters, and M. Yagmurcukardes, "Single-layer Janus black arsenic-phosphorus (b-AsP): optical dichroism, anisotropic vibrational, thermal, and elastic properties," *Physical Review B*, vol. 101, no. 13, article 134102, 2020.

[32] A. Kandemir and H. Sahin, "Janus single layers of In_2SSe: a first-principles study," *Physical Review B*, vol. 97, no. 15, p. 7, 2018.

[33] H. Yang, Y. Ma, S. Zhang, H. Jin, B. Huang, and Y. Dai, "GeSe@SnS: stacked Janus structures for overall water splitting," *Journal of Materials Chemistry A*, vol. 7, no. 19, pp. 12060–12067, 2019.

[34] G. Eda, H. Yamaguchi, D. Voiry, T. Fujita, M. Chen, and M. Chhowalla, "Photoluminescence from chemically exfoliated MoS_2," *Nano Letters*, vol. 11, no. 12, pp. 5111–5116, 2011.

[35] J. Bardeen, "Surface states and rectification at a metal semiconductor contact," *Physics Review*, vol. 71, no. 10, pp. 717–727, 1947.

[36] V. Heine, "Theory of surface states," *Physics Review*, vol. 138, no. 6A, pp. A1689–A1696, 1965.

[37] S. Shi, Z. Sun, and Y. H. Hu, "Synthesis, stabilization and applications of 2-dimensional 1T metallic MoS_2," *Journal of Materials Chemistry A*, vol. 6, no. 47, pp. 23932–23977, 2018.

[38] Y. Liu, P. Stradins, and S. H. Wei, "Van der Waals metal-semiconductor junction: weak Fermi level pinning enables effective tuning of Schottky barrier," *Science Advances*, vol. 2, no. 4, article e1600069, 2016.

[39] R. Quhe, Y. Wang, M. Ye et al., "Black phosphorus transistors with van der Waals-type electrical contacts," *Nanoscale*, vol. 9, no. 37, pp. 14047–14057, 2017.

[40] G. Kresse and J. Furthmuller, "Efficiency of ab-initio total energy calculations for metals and semiconductors using a plane-wave basis set," *Computational Materials Science*, vol. 6, no. 1, pp. 15–50, 1996.

[41] G. Kresse and J. Furthmüller, "Efficient iterative schemes forab initiototal-energy calculations using a plane-wave basis set," *Physical Review B*, vol. 54, no. 16, pp. 11169–11186, 1996.

[42] J. P. Perdew, K. Burke, and M. Ernzerhof, "Generalized gradient approximation made simple," *Physical Review Letters*, vol. 77, no. 18, pp. 3865–3868, 1996.

[43] P. E. Blöchl, "Projector augmented-wave method," *Physical Review B*, vol. 50, no. 24, pp. 17953–17979, 1994.

[44] G. Kresse and D. Joubert, "From ultrasoft pseudopotentials to the projector augmented-wave method," *Physical Review B*, vol. 59, no. 3, pp. 1758–1775, 1999.

[45] A. Tkatchenko and M. Scheffler, "Accurate molecular van der Waals interactions from ground-state electron density and free-atom reference data," *Physical Review Letters*, vol. 102, no. 7, article 073005, 2009.

[46] T. Shen, J.-C. Ren, X. Liu, S. Li, and W. Liu, "Van der Waals stacking induced transition from Schottky to Ohmic contacts: 2D metals on multilayer InSe," *Journal of the American Chemical Society*, vol. 141, no. 7, pp. 3110–3115, 2019.

[47] X. Liu, J.-C. Ren, S. Zhang, M. Fuentes-Cabrera, S. Li, and W. Liu, "Ultrahigh conductivity in two-dimensional InSe via remote doping at room temperature," *Journal of Physical Chemistry Letters*, vol. 9, no. 14, pp. 3897–3903, 2018.

[48] M. Brandbyge, J.-L. Mozos, P. Ordejón, J. Taylor, and K. Stokbro, "Density-functional method for nonequilibrium electron transport," *Physical Review B*, vol. 65, no. 16, article 165401, 2002.

[49] M. Kan, J. Y. Wang, X. W. Li et al., "Structures and phase transition of a MoS_2 monolayer," *Journal of Physical Chemistry C*, vol. 118, no. 3, pp. 1515–1522, 2014.

[50] F. Raffone, C. Ataca, J. C. Grossman, and G. Cicero, "MoS_2 enhanced T-phase stabilization and tunability through alloying," *Journal of Physical Chemistry Letters*, vol. 7, no. 13, pp. 2304–2309, 2016.

[51] E. H. Rhoderick, "Metal-semiconductor contacts," *IEE Proceedings I - Solid-State and Electron Devices*, vol. 129, no. 1, p. 1, 1982.

[52] Z. Zhang, K. Yao, Y. Liu et al., "Quantitative analysis of current–voltage characteristics of semiconducting nanowires: decoupling of contact effects," *Advanced Functional Materials*, vol. 17, no. 14, pp. 2478–2489, 2007.

[53] F. Ahmed, M. S. Choi, X. Liu, and W. J. Yoo, "Carrier transport at the metal–MoS_2 interface," *Nanoscale*, vol. 7, no. 20, pp. 9222–9228, 2015.

[54] B. K. Sarker and S. I. Khondaker, "Thermionic emission and tunneling at carbon nanotube–organic semiconductor interface," *ACS Nano*, vol. 6, no. 6, pp. 4993–4999, 2012.

[55] S. G. Louie and M. L. Cohen, "Self-consistent pseudopotential calculation for a metal-semiconductor interface," *Physical Review Letters*, vol. 35, no. 13, pp. 866–869, 1975.

[56] C. Gong, L. Colombo, R. M. Wallace, and K. Cho, "The unusual mechanism of partial Fermi level pinning at metal–MoS_2 interfaces," *Nano Letters*, vol. 14, no. 4, pp. 1714–1720, 2014.

[57] C. Si, Z. Lin, J. Zhou, and Z. Sun, "Controllable Schottky barrier in GaSe/graphene heterostructure: the role of interface dipole," *2D Materials*, vol. 4, no. 1, article 015027, 2017.

[58] F. Mott Nevill, "The theory of crystal rectifiers," *Proceedings of the Royal Society of London Series A: Mathematical and Physical Sciences*, vol. 171, no. 944, pp. 27–38, 1939.